Detection and Localization of Series Arc Faults in DC Microgrids using Kalman Filter

Kaushik Gajula, *Student Member, IEEE*, and Luis Herrera, *Member, IEEE*Department of Electrical Engineering

University at Buffalo

Abstract—— DC networks are becoming more popular in a wide range of applications. However, the difficulty in detecting and localizing a high impedance series arc fault presents, a major challenge slowing the wider deployment of dc networks/microgrids. In this paper, a Kalman Filter (KF) based algorithm to monitor the operation of a dc microgrid by estimating the line admittances and consequently detecting/localizing series arc faults is introduced. The proposed algorithm uses voltage and current samples from the nodes in the distribution network to estimate the line admittances. By determining these values, it is possible to quickly isolate the faulted section and reconfigure the network after a fault occurs. Since, the disturbance caused by a high impedance series arc fault spreads across almost the entire microgrid, the KF algorithm is structured to detect the faulted line in the grid with precision. Simulation and Control Hardware in the Loop (CHIL) results are presented demonstrating the feasibility of implementation.

Index Terms—Kalman filter, dc microgrid, series arc fault, parameter estimation, fault detection, fault localization.

I. INTRODUCTION

S the adoption of dc microgrids [1]–[3] continue to increase in Electric Vehicles (EVs) [4], [5], More Electric Aircraft (MEA) [6], electric ships [7]–[9], and charging stations [10], [11], it is extremely important to analyze and detect any dangers or faults that occur while operating these networks. One type of fault which is difficult to detect and localize in dc systems is the series arc fault [12]. The fault occurs when a dc voltage difference exists across an air gap in series with the circuit. It is typically caused by loose connections, line degradation, etc. and can be mistaken for load change due to its low fault current. The lack of zero voltage crossings in a dc system further prevents this type of fault from naturally extinguishing (as opposed to ac networks).

In recent years, it has been shown that the series arc's disturbance/noise can travel to adjacent lines and trigger detectors in multiple sections of a network [13]–[15]. In order to mitigate this problem and accurately detect the faulted line, [16] and [17] propose parameter estimation techniques for a single line based on continuous time (gradient method) and in discrete time (Recursive Least Squares (RLS), Kalman Filter (KF)) methods respectively. However, in both these papers fault detection was obtained by estimating the line resistances and inductances locally, i.e. over each line independently. With regards to series arc fault detection, [18] uses a band pass filter to decrease the low frequency grid voltage fluctuation caused by the load variations and high frequency system noises. By measuring voltage drop on the load side, a decision is

taken to disconnect the load from the circuit. Nevertheless, since the series arc noise can travel to adjacent lines in a microgrid, multiple detectors can trip using this technique [19]. A KF based approach is used to detect a fault on a PV circuit in [20]. Here the signal is studied on the basis of its component frequencies and Signal to Noise Ratio (SNR) to detect the fault. However, localization (locating the line affected by series arc fault) is not addressed. Fault detection by using an algorithm based on machine learning is shown in [21]. The algorithm is considerably complex as it is layer based and needs to be trained by test data to detect the series arc signatures before being deployed in real time. Although it has high detection accuracy, localization of series fault on a large network is not explored. Moreover, on a dynamic topology with variable current flow directions based on power demands, the machine learning algorithm would require more training. Therefore, it can be seen that most detection techniques use local measurements (current and/or voltage) within a single line to detect a series arc fault. However, multiple detectors could be triggered since the fault noise can spread through the system. Thus, it is important to consider a centralized methodology which analyzes the entire network. Additionally, a centralized approach takes advantage of the different sensors available in a microgrid, leading to a better and more accurate estimation of the parameters (line admittances) being used to detect and localize a series arc fault.

In ac power systems, line admittance and topology estimation has been studied in recent years. In [22], estimation of the topology with admittance parameters in a poly-phase distribution network using the voltage and current from all nodes, is presented based on the Least Absolute Shrinkage and Selection Operator (LASSO) method. Furthermore, a convex optimization relaxation for LASSO was introduced which is capable to detect and localize critical events. The paper [23] tests the Newton Method (NM) and the Approximate Newton Method (ANM) to estimate the line admittances of an ac network by using nodal voltage and injected current measurements while including measurement noise. In [24] least squares method is implemented to estimate line admittances in a three node power grid. Group LASSO algorithm is used to estimate a mesh or a radial topology for medium and low voltage distribution grids by using smart meter measurements [25]. Sparse data of current and voltage measurements to estimate a distribution grid's topology has always been a concern. To address this issue [26] suggests, an optimal placement of meters can help lower the number of sensors

deployed and maintain full observability of the distribution grid. In [27], a physical-probabilistic-network (PPN) model for inferring overall operation mode of distribution networks is presented. On the basis of input and output noise correlation and nonlinear power flow equations, a model that considers the measurement errors in its variables is formulated as a Maximum Likelihood Estimation (MLE) problem for joint topology and line parameter estimation in [28]. Admittance based detection has been proposed in dc systems for short circuit (parallel) faults [29]. In this case, a drop in resistance (increase in admittance) is used to detect and isolate a short circuit fault on a Medium Voltage Direct Current (MVDC) system within 20 ms.

Application of Kalman Filter on dynamic systems can be notably seen in aerospace, transportation, navigation, stock market predictions and others. The KF has been further improved into Extended Kalman Filter (EKF) and Unscented Kalman Filter (UKF) in order to incorporate estimations of unobservable variables in nonlinear systems. In [30], [31], an application of EKF coupled with robust control to estimate the dynamic state variables of a power system is presented. A new variant of UKF is implemented and compared to the existing versions of UKF and the EKF in power system dynamic state estimation [32]. A robust generalized maximum likelihood based KF is implemented to estimate the rotor angle and speed of synchronous generators in [33]. The paper [34] applies the Ensemble Kalman Filter to detect and localize a fault on transmission lines. The paper [35] presents a self-tuning control technique which adaptively estimates the discrete time transfer function of a dc-dc buck converter by using the KF and a M-Max partial adaptive filtering technique to compute the controller gains online.

Motivated by the recent developments in ac network topology estimation, this paper presents a KF based algorithm to estimate the admittance matrix (hence line admittances) for a dc microgrid. The admittance matrix is introduced as a dynamic system to KF. The main contributions of our work include, formulation and application of KF and Adaptive Kalman Filter (AKF) algorithms for series arc fault detection and localization through line admittance estimation, which are not susceptible to normal transient operations on a dc microgrid. The proposed method is operated at each iteration/sample which can help in faster series arc fault detection and can be easily implemented on any dc based microgrid such as EVs, MEA, electric ships, charging stations, space vehicles etc. where, the detection and localization of series arc fault needs to be achieved as fast as possible. It is shown that the AKF is a suitable choice for series arc fault detection and localization with very good performance.

This paper is structured as follows. In Section II, a description of dc microgrid is presented. In Section III, the KF and AKF algorithms are described in detail and a description of the cases considered to evaluate these algorithms along with their respective simulation results are shown in Section IV. Furthermore, Section V presents Control Hardware In Loop (CHIL) results using the Opal RT to run KF/AKF and the Plecs RT Box to simulate the network. Finally, a conclusion and future work are stated in Section VI.

The following notations are used in this paper. For a matrix $A \in \mathbb{R}^{m \times n}$, its vectorization is denoted as $\text{vec}(A) = (A_{11}, \cdots, A_{m1}, A_{12}, \cdots, A_{m2}, \cdots, A_{1n}, \cdots, A_{mn})^T$. The symbol \otimes denotes the Kronecker product of two matrices. An N-dimensional Identity matrix is represented by, \mathcal{I}_N .

II. SYSTEM DESCRIPTION

In this section, a typical dc microgrid is described on the basis of its voltage and current measurements to estimate its line admittances.

A. Microgrid Description

A typical dc microgrid is composed of loads, generators and distribution lines. The dc generators can be based on renewable energy sources (e.g. wind, solar, etc.), energy storage, and/or fuel based engines (main energy source in aircrafts or electric ships). Both generators and loads are connected to the network through dc/dc converters. When the load is actively regulated, it is typically classified as nonlinear Constant Power Load (CPL) [36]. The energy sources commonly share power using droop control [37], although decentralized and distributed techniques have been proposed recently [38]. Moreover, voltage and current sensors are assumed to be installed at each node in the network.

In steady state, a dc microgrid can be described by the following nodal equations:

$$I(k) = Y(k) V(k) \tag{1}$$

where, $I(k) \in \mathbb{R}^N$ and $V(k) \in \mathbb{R}^N$ are the vectors of injected current and voltage measurements respectively, obtained from all the nodes at every k^{th} sample, i.e.

$$I(k)^{T} = \begin{pmatrix} I_{1}(k) & I_{2}(k) & \cdots & I_{N}(k) \end{pmatrix}$$

 $V(k)^{T} = \begin{pmatrix} V_{1}(k) & V_{2}(k) & \cdots & V_{N}(k) \end{pmatrix},$ (2)

and $Y \in \mathbb{R}^{N \times N}$ is the admittance matrix.

In order to use parameter identification techniques to estimate the admittance matrix, it is necessary to place the system (1) in linear regression form as follows:

$$y(k) = H(k) x(k) + v(k).$$
 (3)

Where, y(k) is the output (related to the sensors in a network), x(k) contains the parameters to be estimated (e.g. admittance matrix elements), H(k) is the basis matrix, and v(k) is the measurement noise. This implies the need to vectorize the admittance matrix Y, to be contained in the unknown vector of states x(k). Using (1), we can obtain the following:

$$\operatorname{vec}\left(I(k)\right) = \operatorname{vec}\left(Y(k)V(k)\right). \tag{4}$$

Which can be simplified as [22]:

$$\underbrace{I(k)}_{y(k)} = \underbrace{\left(V(k)^T \otimes \mathcal{I}_N\right)}_{\triangleq H_Y(k)} \underbrace{\operatorname{vec}\left(Y(k)\right)}_{x_Y(k)}.$$
 (5)

However, as the admittance matrix Y is symmetric and the elements along the diagonal are sign opposite to the sum of the elements along the respective row or column (assuming there are no line to ground resistances), the dimension of vector

x(k) can be reduced to contain only the elements in the lower triangular matrix without considering the diagonal elements. This allows the number of parameters being estimated for an $(N \times N)$ dimensional admittance matrix Y to be $\frac{[N][N-1]}{2}$, which is a significant reduction. Therefore, for an admittance matrix of the form:

$$Y(k) = \begin{pmatrix} Y_{1,1}(k) & Y_{1,2}(k) & \cdots & Y_{1,N}(k) \\ Y_{2,1}(k) & Y_{2,2}(k) & \cdots & Y_{2,N}(k) \\ \vdots & \vdots & \ddots & \vdots \\ Y_{N,1}(k) & Y_{N,2}(k) & \cdots & Y_{N,N}(k) \end{pmatrix}.$$
 (6)

The state vector for an unknown network topology becomes:

$$x_{\text{utop}}^T = (Y_{2,1} \quad Y_{3,1} \quad \cdots \quad Y_{3,2} \quad Y_{4,2} \quad \cdots \quad Y_{N,N-1})$$
 (7)

and equation (1) can be further simplified as:

$$y(k) = \left[\left(V(k)^T \otimes \mathcal{I}_N \right) Q_Y \right] x_{\text{utop}}(k). \tag{8}$$

The matrix Q_Y is defined such that $\mathrm{vec}\,(Y(k)) = Q_Y x_{\mathrm{utop}}(k)$. The algorithm for obtaining the Q_Y matrix for any N bus network is shown in Table III in the appendix.

Lastly, as the topology for dc microgrids is generally defined, the number of unknowns in (7) can be further reduced by eliminating those elements for which a line does not exists. Therefore, the system for parameter estimation is defined as:

$$y(k) = \underbrace{\left[\left(V(k)^T \otimes \mathcal{I}_N\right) Q_Y M\right]}_{H(k)} x. \tag{9}$$

Where $H(k) \triangleq [(V(k)^T \otimes \mathcal{I}_N) Q_Y M]$, M satisfies $\text{vec}(Y) = Q_Y M x$, and x contains only the line admittance elements that are present in the network.

The detection and localization of series arc fault (high impedance change in line) can then be performed by the estimation of the line admittance values in x. The values of the line admittances will be estimated at every sample "k".

B. Series Arc Fault

The main type of fault considered in this paper is the series arc due to its difficulty in detection and localization. Series arc fault is defined as an unintended power discharge between two conductors in series with the circuit, shown in Fig. 1. As the air in the gap becomes ionized by the high relative charge on either side of the conductors, it allows for the current to flow by generating heat and can eventually cause fires. This gap can be caused by loose or chafed wire connections [12].

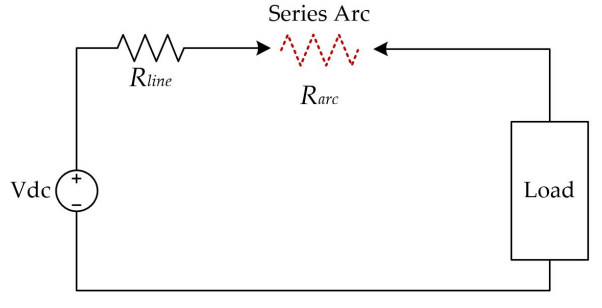


Fig. 1. Example of series arc fault on a line.

TABLE I. Kalman Filter Algorithm [39].

Model:	$x(k+1) = \mathcal{I}x(k) + w(k), \ w(k) \sim \mathcal{N}(0, \ Q(k))$ $y(k) = H(k)x(k) + v(k) \ v(k) \sim \mathcal{N}(0, \ R(k))$
Initialize:	$P^{-}(0) = E\left[(\hat{x}(0) - x)(\hat{x}(0) - x)^{T} \right]$
	$\hat{x}(0) = E[x]$
Gain:	$K(k) = P^{-}(k)H^{T}(k) [H(k)P^{-}(k)H^{T}(k) + R]^{-1}$
Update:	$P^{+}(k) = P^{-}(k) - K(k)H(k)P^{-}(k)$
	$\hat{x}^{+}(k) = \hat{x}^{-}(k) + K(k) \left[y(k) - H(k)\hat{x}^{-}(k) \right]$
Propagation:	$P^{-}(k+1) = \mathcal{I}P^{+}(k)\mathcal{I}^{T} + Q$
	$\hat{x}^-(k+1) = \mathcal{I}\hat{x}^+(k)$

The detection of series arc is difficult since the fault current is relatively low, compared to parallel faults. Moreover, the noise caused by the arc can travel to adjacent lines and trigger detectors in multiple sections of a network [15]. From Fig. 1, it can be seen that during a series arc fault, a resistance is added in series with the line/circuit.

III. KALMAN FILTER BASED ADMITTANCE ESTIMATION

In this section, the derivation of the KF is described in accordance with the system in (9) to estimate the admittances in dc microgrid with known topology.

A. Kalman Filter Algorithm

We first formulate the state vector x(k) as a discrete linear system of the form,

$$x(k) = F(k-1)x(k-1) + G(k-1)u(k-1) + w(k-1).$$
(10)

Where, w(k) is the process noise and u(k) contains the inputs. However, for parameter estimation, (10) is simplified to:

$$x(k) = \mathcal{I}x(k-1) + w(k-1)$$
(11)

Therefore, $F = \mathcal{I}$ is an identity matrix of appropriate dimension and the input vector u(k) is zero. Defining $\hat{x}(k)$ as the estimates of x(k), we can define the following:

$$P(k) \triangleq E\left[(\hat{x}(k) - x)(\hat{x}(k) - x)^T \right]$$
 (12)

$$R(k) \triangleq E\left[v(k)v(k)^{T}\right] \tag{13}$$

$$Q(k) \triangleq E\left[w(k)w(k)^{T}\right]. \tag{14}$$

Where, P(k), R(k), and Q(k) denote the error, measurement noise, and the process noise covariance matrices respectively. The mean of the process and measurement noise is assumed to be zero.

The matrix P is initialized as $P(0) = E\left[(\hat{x}(0) - x)(\hat{x}(0) - x)^T\right]$ which updates over every iteration. The measurement and process noise covariance, R and Q, are typically fixed. In this paper, $R = n \mathcal{I}$ and $Q = p \mathcal{I}$, where n and p are constants.

The KF minimizes the sum of the squares of the a posteriori errors at time k, i.e. $Tr(P(k)^+)$, to derive the gain matrix:

$$K(k) = P^{-}(k)H^{T}(k)[H(k)P^{-}(k)H^{T}(k) + R]^{-1}.$$
 (15)

Where, $P(k)^-$ denotes the a priori error covariance estimate, computed as follows:

$$P^{-}(k) = F(k-1)P^{+}(k-1)F^{T}(k-1) + Q.$$

$$\Rightarrow P^{-}(k) = \mathcal{I}P^{+}(k-1)\mathcal{I}^{T} + Q.$$
(16)

Similarly, the a priori state estimate is given by:

$$\hat{x}^{-}(k) = F(k-1)\hat{x}^{+}(k-1) + G(k-1)u(k-1)$$

$$\Rightarrow \hat{x}^{-}(k) = \mathcal{I}\hat{x}^{+}(k-1)$$
(17)

Finally, at time k, the optimal estimate is:

$$\hat{x}^{+}(k) = \hat{x}^{-}(k) + K(k) \left[y(k) - H(k)\hat{x}^{-}(k) \right]$$
 (18)

$$P^{+}(k) = P^{-}(k) - K(k)H(k)P^{-}(k)$$
(19)

The steps involved in the implementation of the KF are summarized in Table I.

B. Adaptive Kalman Filter

As described in the previous subsection, the process noise covariance, Q(k), is typically assumed to be constant. However, since the actual process covariance is difficult to know a priori, it is possible to estimate it iteratively [40]–[42]. The Adaptive Kalman Filter (AKF) evaluates this matrix at every k^{th} sample. Considering x_i to be the i^{th} element of x, this can be accomplished as follows:

$$w_i \triangleq \hat{x}_i(k)^+ - \hat{x}_i(k)^- \tag{20}$$

$$Q(k) = \lambda \operatorname{diag}\left[\left[w_1 \right]^2; \left[w_2 \right]^2; \left[w_3 \right]^2; \cdots \right].$$
 (21)

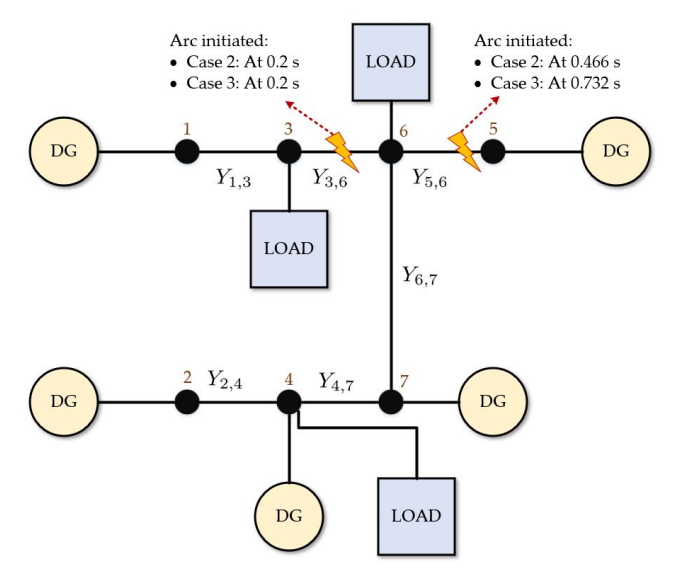
Where, λ is a positive gain. The equation (21) is added prior to the propagation phase of the Kalman Filter which changes the error covariance matrix at propagation phase to:

$$P^{-}(k) = F(k-1)P^{+}(k-1)F^{T}(k-1) + Q(k-1).$$

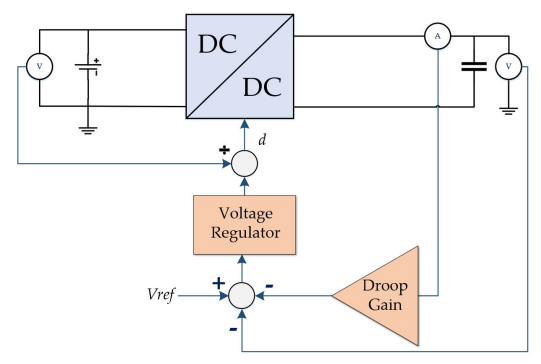
It will be shown in the case study section that estimating the process covariance, Q(k), has better performance than if it is considered to be constant in the regular KF.

TABLE II. DC microgrid parameters

Line	Length	Inductance	Resistance	Admittance
	(miles)	(H)	(Ω)	(U)
(1,3)	0.1	1.6e-4	0.12	8.33
(2,4)	0.1	1.6e-4	0.12	8.33
(3,6)	0.125	2e-4	0.15	6.67
(4,7)	0.125	2e-4	0.15	6.67
(5,6)	0.15	2.4e-4	0.18	5.55
(6,7)	0.05	8e-5	0.06	16.67



(a) The 7 node dc microgrid used in the case studies.



(b) Schematic of voltage regulator and droop control for each distributed source.

Fig. 2. DC microgrid considered in the case studies and closed loop feedback control structure for one source.

IV. CASE STUDY AND OFFLINE SIMULATION RESULTS

In this section, we illustrate the ability of the proposed algorithms in estimation of line admittances, fault detection/localization, and robustness to nominal operation conditions. The dc microgrid shown in Fig. 2a was simulated using Matlab Simpower Systems. The simulation time step is 10 μ s while, the total simulation time is 1 s. The sensors at every node were sampled at a rate of 100 μ s. Each generator and load is connected to the network through a buck converter. The inductance and capacitance of each converter are 1 mHand 1 mF respectively. The nominal dc voltage of the network is assumed to be 390 V. The input voltage of the generator converters is 600 V. The generators share power through the traditional droop control [37]. An example of the controller for one source is shown in Fig. 2b. The network includes five sources at nodes 1, 2, 4, 5 and 7 and three loads at nodes 3, 4 and 6. The initial value of the load currents at nodes 3, 4, and 6 are 175 A, 150 A, and 125 A respectively, with an output load side voltage of 220 V. The total load power is 100 kW.

The resistance and inductance values for each line are shown in Tab. II. After a series arc fault occurs, the lines $Y_{3,6}$ and $Y_{5,6}$, increase their line resistances from 0.15 Ω to 1.65 Ω and from 0.18 Ω to 1.98 Ω respectively, to imitate the behavior

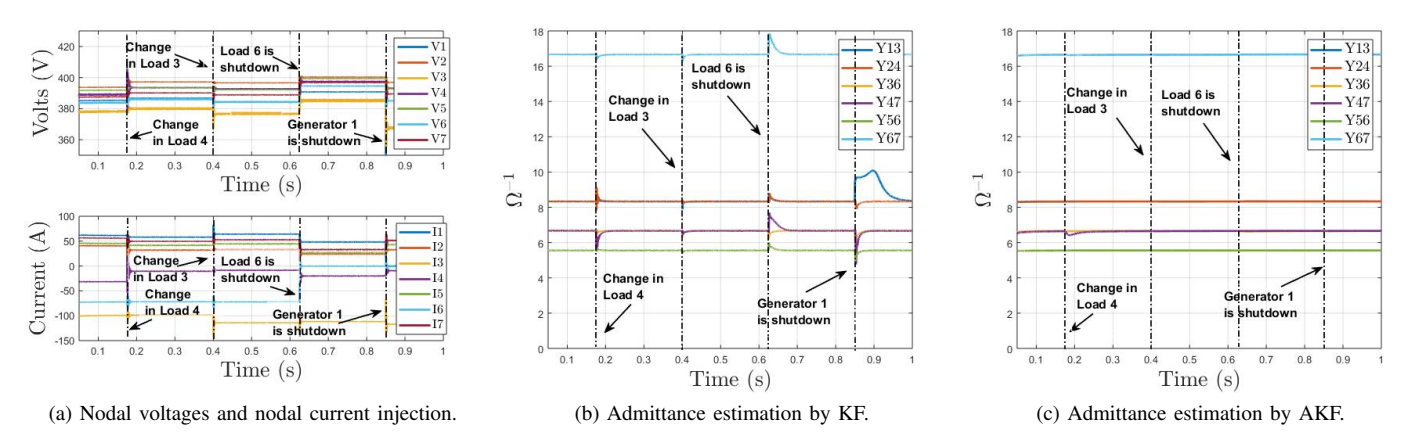


Fig. 3. Simulation results for Case 1. Change in Load 4's current occurs at t = 0.175 s, change in Load 3's current occurs at t = 0.4 s, Load 6 is turned off at t = 0.625 s and Generator 1 is turned off at t = 0.85 s.

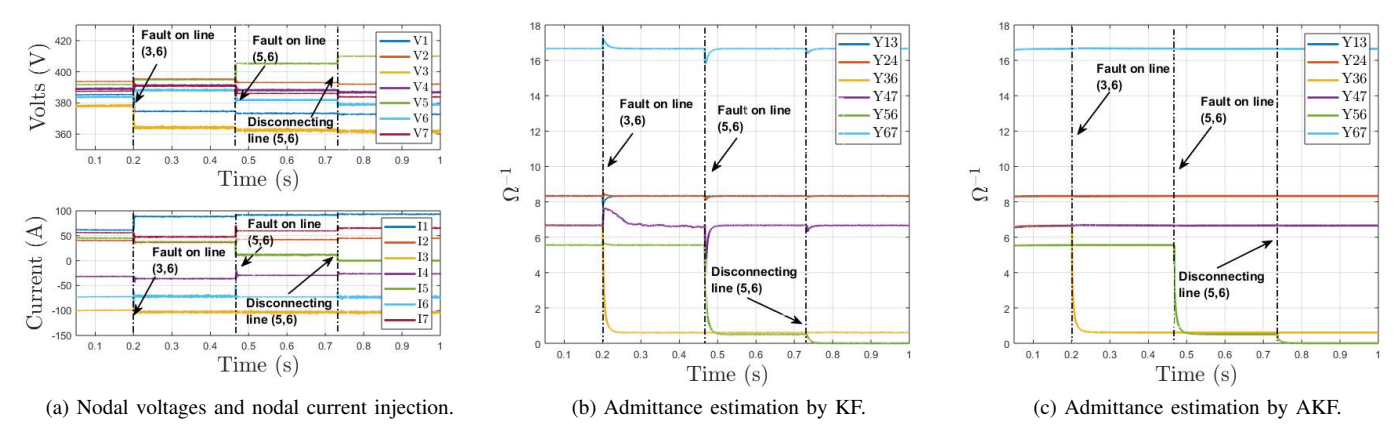


Fig. 4. Simulation results for Case 2. The first series are occurs at t = 0.2 s on line (3,6) followed by a second high impedance fault occurs at t = 0.466 s on line (5,6) and then, line (5,6) is disconnected at t = 0.732 s.

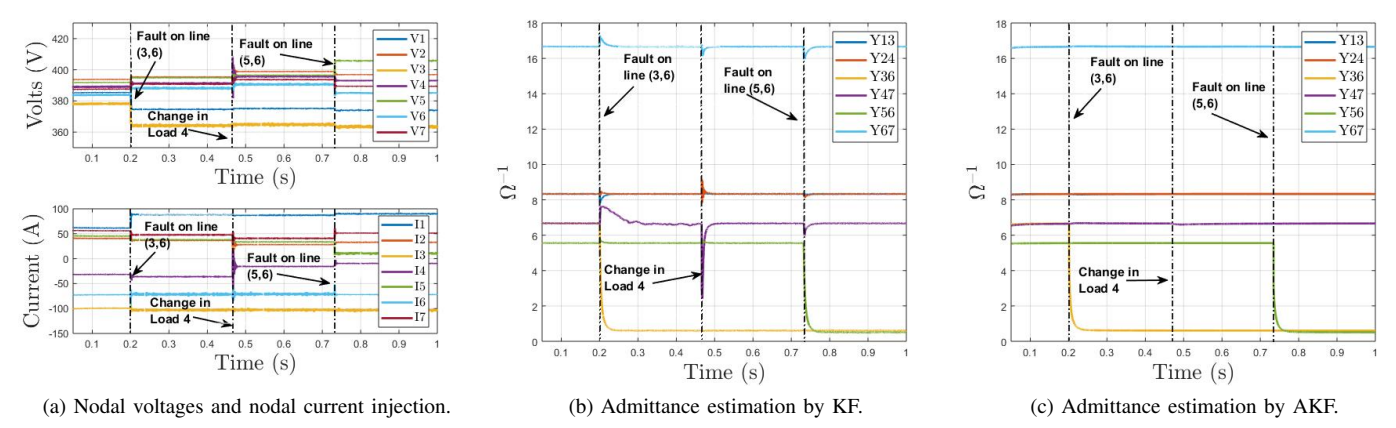


Fig. 5. Simulation results for Case 3. First series arc occurs at t = 0.2 s on line (3,6) followed by a current change by Load 4 at t = 0.466 s and a second series arc fault occurs at t = 0.732 s on line (5,6).

of the series fault in line. The KF/AKF algorithms are then tested over the following three cases:

- <u>Case 1</u> (Nominal Operation): Change in Load 4 at t = 0.175 s, change in Load 3 at t = 0.4 s, Load 6 is switched off at t = 0.625 s and Generator 1 is turned off at t = 0.85 s.
- Case 2: Series arc fault on line (3,6) at t = 0.2 s followed
- by another series arc fault on line (5,6) at t = 0.466 s and disconnection of line (5,6) at t = 0.732 s.
- <u>Case 3</u>: Series arc fault on line (3,6) at t = 0.2 s, change in Load 4 at t = 0.466 s, followed by another series arc fault on line (5,6) at t = 0.732 s.

A. Case 1

In this case, KF and AKF are used to estimate the line admittances in the presence of load and generator changes. The nodal voltages and injection currents at each bus are shown in Fig. 3a. The estimation of line admittances using KF is shown in Fig. 3b. Fig. 3c shows the estimation of line admittances by AKF. Since there was no fault during this case, the line admittances should not be affected by the source/load changes. However, using KF, it can be clearly seen that these events cause small transients in the admittance estimation as shown in Fig. 3b. The proposed AKF technique shows a better response as seen in Fig. 3c. Only a small transient is seen in the admittance estimation of line (4,7) during a change in load 4.

B. Case 2

In this case, the proposed methods are tested during multiple line faults and one line disconnection. The overall results are shown in Fig. 4. The nodal voltages and current injections are shown in Fig. 4a. The first series arc fault occurs on line (3,6) at t=0.2 s and a second series arc occurs on line (5,6) at t=0.466 s. The admittance on line (3,6) drops from 6.67 \mho to 0.6 \mho which is shown by the yellow line in Figs. 4b, 4c. Similarly, the line admittance on line (5,6) drops from 5.55 \mho to 0.5 \mho shown by the green line in Figs. 4b, 4c. Furthermore, line (5,6) is disconnected at t=0.732 s which can be seen by the green line going to zero in Figs. 4b, 4c.

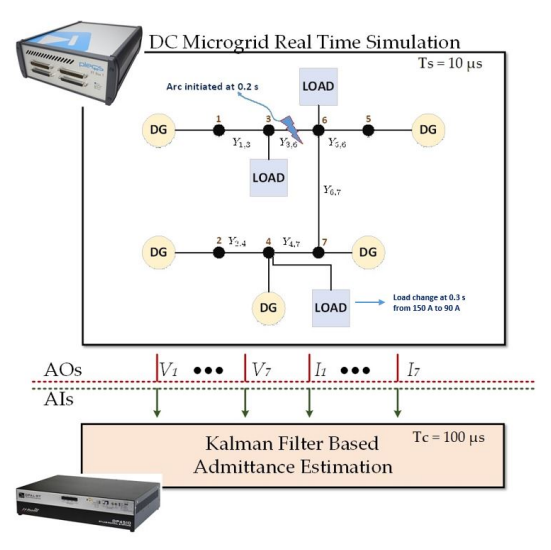
It can be clearly seen that series arc fault occurrence on the specified lines could cause a very small transient in the admittance estimation of the other lines while using KF. Whereas, we observe no such transience in line admittance estimation while using the AKF. However, it should be noted that both KF and AKF are capable to detect and localize series arc faults.

C. Case 3

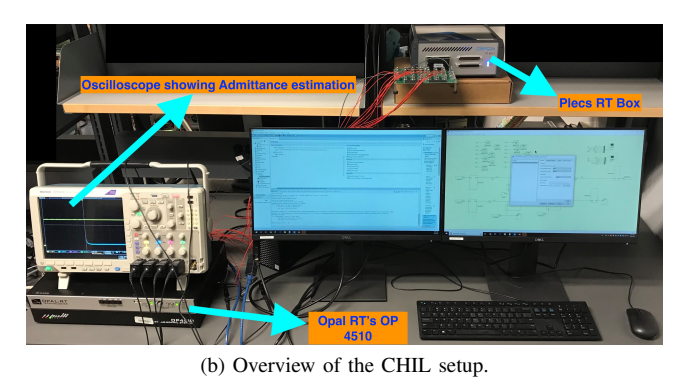
In this case, two series faults are initiated with one load change in between them. The simulation results are shown in Fig. 5. The nodal voltages and current injections in the network are shown in Fig. 5a. The first series arc fault occurs on line (3,6) at t = 0.2 s. This is followed by a change in Load 4's current from 150 A to 90 A at t = 0.466 s which can be shown by the purple line in Fig. 5a. A second series arc fault is set to occur on line (5,6) at t = 0.732 s. The admittance on line (3,6) drops from 6.67 \mho to 0.6 \mho during the first fault, shown by the yellow line in Figs. 5b, 5c. Similarly, the admittance on line (5,6) drops from 5.55 \mho to 0.5 \mho on the occurrence of series arc fault at t = 0.732 s, which is shown by the green line in Figs. 5b, 5c. Using KF, it can be seen that the occurrence of series arc faults affect the line estimation of adjacent lines as well. However, the proposed AKF method presents better performance and robustness to nominal load changes.

V. CONTROL HARDWARE IN LOOP RESULTS

In this section, the dc microgrid used in the offline simulation results and shown in Fig. 2a is implemented in real



(a) Control Hardware in the Loop (CHIL) platform. The dc microgrid is simulated in real time using Plecs and the KF based admittance estimation is implemented in an Opal RT system.



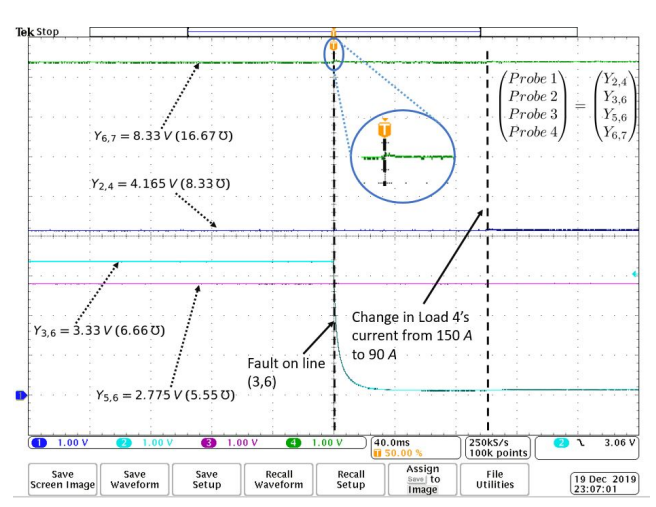
1, 6 : 1, 17 1 1 :

Fig. 6. CHIL results of series arc in line $Y_{3,6}$ and admittance estimation.

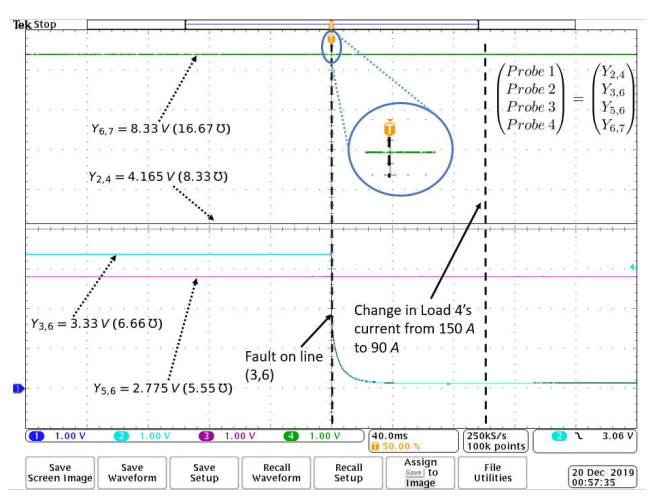
time using Plecs RT Box [43]. The simulation is executed at a time step of $T_s=10~\mu s$. However, this time step was achieved by simplifying the loads to Constant Current Loads (CCLs) operating at 390 V, while the sources are still based on detailed buck converter models (Fig. 2b). The high impedance series are occurs only on line (3,6) at t=0.2 s followed by a change in current drawn by Load 4 at t=0.3 s from an initial 150 A to 90 A.

The KF algorithm (general and adaptive) were implemented in an Opal RT system [44]. The time step of the algorithms is $T_c=100~\mu s$. The nodal voltages and nodal current injections are transferred from the model simulated by PLECS RT Box into the OPAL RT for line admittance estimation using the corresponding analog I/Os. The line admittances are then displayed on an oscilloscope connected to the OPAL RT's Analog Output (AO) slot. The overall platform is described and shown in Figs. 6a and 6b.

The results of the admittance estimation are shown in Figs. 7a and 7b by KF and AKF respectively. In these graphs, only four admittances are observed: Y_{24} , Y_{36} , Y_{56} , and Y_{67} . As can be seen by the light blue trace (Y_{36}) , there is a large decrease in admittance, from 6.67 \mho (3.33 V) to 0.60 \mho ,



(a) Line admittances (four) during series arc on line (3,6) at t=0.2 s followed by a change in Load 4's current from 150 A to 90 A - Kalman Filter.



(b) Line admittances (four) during series arc on line (3,6) at t=0.2 s followed by a change in Load 4's current from 150 A to 90 A - Adaptive Kalman Filter.

Fig. 7. CHIL results by Kalman Filter and Adaptive Kalman Filter.

indicating a large increase from $0.15~\Omega$ to $1.65~\Omega$ in the line resistance. Thus, it can be inferred that a high impedance fault occurred on this line. It can be seen that the algorithm can quickly estimate the right value during a fault. Moreover, the estimation of the other line admittances are not significantly affected by this change. A magnified picture within the graphs show the behavior on $Y_{3,6}$'s estimation during the fault. A small transient in the admittance estimation can be seen in Fig. 7a, whereas the line (3,6) estimated in Fig. 7b (AKF) is not affected. This further demonstrates the advantage of AKF over the regular KF. In addition, at $t=0.3~\mathrm{s}$ a change in current demand at Load 4 is added and does not affect the line admittance estimates significantly, especially the AKF.

VI. CONCLUSION AND FUTURE WORK

A centralized application of Kalman Filter and Adaptive Kalman Filter for series are fault detection and localization are demonstrated on a dc microgrid. The formulation of KF/AKF for any N node grid is presented in combination with steps to express the admittance equation in linear regression form.

The KF based estimation algorithms are then demonstrated over three cases to include the conditions that imitate a regular operation of a dc microgrid. The results illustrate an accurate estimation of microgrid's line admittances followed by a quick detection and localization of two independent series arc faults. CHIL results were obtained by interfacing the Plecs RT Box (simulating the dc microgrid) and the Opal RT's OP 4510 (KF based estimation), demonstrating the detection/localization performance for high impedance series arc faults.

For future work, the entire dc microgrid will be implemented using actual hardware. In addition, more in-depth analysis will be conducted for cases where not all node voltage or current injections can be measured. Techniques will be developed and implemented in order to accommodate for these cases.

$\begin{array}{c} {\sf APPENDIX} \\ {\sf ALGORITHM\ TO\ OBTAIN\ } Q_Y \ {\sf MATRIX} \end{array}$

Tab. III presents a pseudo code to generate the Q_Y matrix for any N node dc microgrid. The Q_Y matrix helps reconstruct the vectorized form of the admittance matrix vec (Y) by using only the lower triangular matrix minus the diagonal elements, i.e. vec $(Y) = Q_Y x_{\text{utop}}$, where x_{utop} is defined in (7).

TABLE III. Algorithm to generate the Q_Y matrix used in the vec (Y).

Set
$$\mathbf{p} = \frac{[N][N-1]}{2}$$
 Set $\mathbf{a} = (1,0_{p-1})$ At $j=1$ Set $Q_Y = \begin{pmatrix} -1_{N-1} & 0_{p-N+1} \\ I_{N-1} & 0_{N-1,p-N+1} \end{pmatrix}$ for $j=2,3,4,\cdots,N$ Set $Z=0_p$, $t=0$ and $counter=0$ for $k=0,1,2,3,\cdots,j-2$ Set $t=t+1$ Set $counter=counter+t$ Set $i=\text{Right-Circular-shift } [a,k\times N+j-counter-1]$ Set $Q_Y = \begin{pmatrix} Q_Y \\ i \end{pmatrix}$, $Z = \begin{pmatrix} Z \\ i \end{pmatrix}$ and $D=\text{Sum along each column of } Z$ end Set $\alpha = \begin{pmatrix} 0_{N-j,Nj-N-\frac{j^2}{2}+\frac{j}{2}} & I_{N-j} & 0_{N-j,p-Nj+\frac{j^2}{2}+\frac{j}{2}} \end{pmatrix}$ Set $D=-[D+\text{Sum along each column of } \alpha]$ and $Q_Y=\begin{pmatrix} Q_Y & D & \alpha \end{pmatrix}^T$ end

REFERENCES

- [1] A. Hirsch, Y. Parag, and J. Guerrero, "Microgrids: A review of technologies, key drivers, and outstanding issues," *Renewable and Sustainable Energy Reviews*, vol. 90, pp. 402 411, 2018. [Online]. Available: http://www.sciencedirect.com/science/article/pii/S136403211830128X
- [2] B. Glasgo, I. L. Azevedo, and C. Hendrickson, "Expert assessments on the future of direct current in buildings," *Environmental Research Letters*, vol. 13, no. 7, p. 074004, 2018.
- [3] T. Dragicevic, P. Wheeler, and F. Blaabjerg, DC distribution systems and microgrids. Institution of Engineering and Technology, 2018.
- [4] B. Aluisio, S. Bruno, L. De Bellis, M. Dicorato, G. Forte, and M. Trovato, "Dc-microgrid operation planning for an electric vehicle supply infrastructure," *Applied Sciences*, vol. 9, no. 13, p. 2687, 2019.
- [5] B. Aluisio, M. Dicorato, I. Ferrini, G. Forte, R. Sbrizzai, and M. Trovato, "Optimal sizing procedure for electric vehicle supply infrastructure based on dc microgrid with station commitment," *Energies*, vol. 12, no. 10, p. 1901, 2019.

- [6] G. Buticchi, S. Bozhko, M. Liserre, P. Wheeler, and K. Al-Haddad, "On-board microgrids for the more electric aircraft—technology review," *IEEE Transactions on Industrial Electronics*, vol. 66, no. 7, pp. 5588–5599, July 2019.
- [7] A. Francés-Roger, A. Anvari-Moghaddam, E. Rodríguez-Díaz, J. C. Vasquez, J. M. Guerrero, and J. Uceda, "Dynamic assessment of cots converters-based dc integrated power systems in electric ships," *IEEE Transactions on Industrial Informatics*, vol. 14, no. 12, pp. 5518–5529, Dec 2018.
- [8] M. Al-Falahi, T. Tarasiuk, S. Jayasinghe, Z. Jin, H. Enshaei, and J. Guerrero, "Ac ship microgrids: control and power management optimization," *Energies*, vol. 11, no. 6, p. 1458, 2018.
- [9] A. Haseltalab, M. A. Botto, and R. R. Negenborn, "Model predictive dc voltage control for all-electric ships," *Control Engineering Practice*, vol. 90, pp. 133–147, 2019.
- [10] Y. WU, A. Ravey, D. Chrenko, and A. Miraoui, "A real time energy management for ev charging station integrated with local generations and energy storage system," in 2018 IEEE Transportation Electrification Conference and Expo (ITEC), June 2018, pp. 1–6.
- [11] C. Chen, J. Chen, Y. Wang, S. Duan, T. Cai, and S. Jia, "A price optimization method for microgrid economic operation considering across-time-and-space energy transmission of electric vehicles," *IEEE Transactions on Industrial Informatics*, pp. 1–1, 2019.
- [12] X. Yao, L. Herrera, S. Ji, K. Zou, and J. Wang, "Characteristic study and time-domain discrete- wavelet-transform based hybrid detection of series dc arc faults," *IEEE Transactions on Power Electronics*, vol. 29, no. 6, pp. 3103–3115, June 2014.
- [13] X. Yao, L. Herrera, and J. Wang, "Impact evaluation of series dc arc faults in dc microgrids," in 2015 IEEE Applied Power Electronics Conference and Exposition (APEC), March 2015, pp. 2953–2958.
- [14] X. Yao, "Study on dc arc faults in ring-bus dc microgrids with constant power loads," in 2016 IEEE Energy Conversion Congress and Exposition (ECCE), Sept 2016, pp. 1–5.
- [15] X. Yao, L. Herrera, L. Yue, and H. Cai, "Experimental study of series dc arc in distribution systems," in 2018 IEEE Energy Conversion Congress and Exposition (ECCE), Sept 2018, pp. 1–5.
- [16] L. Herrera and X. Yao, "Parameter identification approach to series dc arc fault detection and localization," in 2018 IEEE Energy Conversion Congress and Exposition (ECCE), Sep. 2018, pp. 497–501.
- [17] K. K. Gajula, L. Herrera, and X. Yao, "Detection of series dc arc on a distribution node using discrete-time parameter identification techniques," in 2019 IEEE Applied Power Electronics Conference and Exposition (APEC), March 2019, pp. 3007–3012.
- [18] A. Shekhar, L. Ramírez-Elizondo, S. Bandyopadhyay, L. Mackay, and P. Bauera, "Detection of series arcs using load side voltage drop for protection of low voltage dc systems," *IEEE Transactions on Smart Grid*, vol. 9, no. 6, pp. 6288–6297, Nov 2018.
- [19] X. Yao, "Study on dc arc faults in ring-bus dc microgrids with constant power loads," in 2016 IEEE Energy Conversion Congress and Exposition (ECCE), Sep. 2016, pp. 1–5.
- [20] M. Ahmadi, H. Samet, and T. Ghanbari, "Kalman filter-based approach for detection of series arc fault in photovoltaic systems," *International Transactions on Electrical Energy Systems*, vol. 29, no. 5, p. e2823, 2019.
- [21] S. Lu, T. Sirojan, B. T. Phung, D. Zhang, and E. Ambikairajah, "Dadegan: An effective methodology for dc series are fault diagnosis in photovoltaic systems," *IEEE Access*, vol. 7, pp. 45831–45840, 2019.
- [22] O. Ardakanian, V. W. S. Wong, R. Dobbe, S. H. Low, A. von Meier, C. Tomlin, and Y. Yuan, "On identification of distribution grids," *CoRR*, vol. abs/1711.01526, 2017. [Online]. Available: http://arxiv.org/abs/1711.01526
- [23] A. Lang, I. Shames, and M. Cantoni, "Structure in total least squares parameter estimation for electrical networks," *IFAC-PapersOnLine*, vol. 51, no. 23, pp. 420–425, 2018.
- [24] A. Lesage-Landry, S. Chen, and J. A. Taylor, "Estimating the frequency coupling matrix from network measurements," arXiv preprint arXiv:1809.08192, 2018.
- [25] Y. Liao, Y. Weng, G. Liu, and R. Rajagopal, "Urban mv and lv distribution grid topology estimation via group lasso," *IEEE Transactions on Power Systems*, vol. 34, no. 1, pp. 12–27, Jan 2019.
- [26] G. Cavraro, A. Bernstein, V. Kekatos, and Y. Zhang, "Real-time identifiability of power distribution network topologies with limited monitoring," *IEEE Control Systems Letters*, vol. 4, no. 2, pp. 325–330, April 2020.
- [27] W. Jiang, J. Chen, H. Tang, S. Cheng, Q. Hu, M. Cai, and S. Rahman, "A physical probabilistic network model for distribution network topology

- recognition using smart meter data," *IEEE Transactions on Smart Grid*, pp. 1–1, 2019.
- [28] J. Yu, Y. Weng, and R. Rajagopal, "Patopa: A data-driven parameter and topology joint estimation framework in distribution grids," *IEEE Transactions on Power Systems*, vol. 33, no. 4, pp. 4335–4347, July 2018.
- [29] P. Cairoli and R. A. Dougal, "Fault detection and isolation in medium-voltage dc microgrids: Coordination between supply power converters and bus contactors," *IEEE Transactions on Power Electronics*, vol. 33, no. 5, pp. 4535–4546, 2017.
- [30] J. Zhao, "Dynamic state estimation with model uncertainties using h_{∞} extended kalman filter," *IEEE Transactions on Power Systems*, vol. 33, no. 1, pp. 1099–1100, Jan 2018.
- [31] J. Zhao, M. Netto, and L. Mili, "A robust iterated extended kalman filter for power system dynamic state estimation," *IEEE Transactions* on *Power Systems*, vol. 32, no. 4, pp. 3205–3216, July 2017.
- [32] J. Qi, K. Sun, J. Wang, and H. Liu, "Dynamic state estimation for multi-machine power system by unscented kalman filter with enhanced numerical stability," *IEEE Transactions on Smart Grid*, vol. 9, no. 2, pp. 1184–1196, March 2018.
- [33] M. Netto and L. Mili, "A robust data-driven koopman kalman filter for power systems dynamic state estimation," *IEEE Transactions on Power Systems*, vol. 33, no. 6, pp. 7228–7237, Nov 2018.
- [34] R. Fan, Y. Liu, R. Huang, R. Diao, and S. Wang, "Precise fault location on transmission lines using ensemble kalman filter," *IEEE Transactions* on *Power Delivery*, vol. 33, no. 6, pp. 3252–3255, Dec 2018.
- [35] M. Ahmeid, M. Armstrong, M. Al-Greer, and S. Gadoue, "Computationally efficient self-tuning controller for dc-dc switch mode power converters based on partial update kalman filter," *IEEE Transactions on Power Electronics*, vol. 33, no. 9, pp. 8081–8090, Sep. 2018.
- [36] L. Herrera, W. Zhang, and J. Wang, "Stability analysis and controller design of dc microgrids with constant power loads," *IEEE Transactions* on Smart Grid, vol. 8, no. 2, pp. 881–888, March 2017.
- [37] J. M. Guerrero, J. C. Vasquez, J. Matas, L. G. de Vicuna, and M. Castilla, "Hierarchical control of droop-controlled ac and dc microgrids - a general approach toward standardization," *IEEE Transactions on Industrial Electronics*, vol. 58, no. 1, pp. 158–172, Jan 2011.
- [38] V. Nasirian, S. Moayedi, A. Davoudi, and F. L. Lewis, "Distributed cooperative control of dc microgrids," *IEEE Transactions on Power Electronics*, vol. 30, no. 4, pp. 2288–2303, April 2015.
- [39] J. L. Crassidis and J. L. Junkins, Optimal estimation of dynamic systems. Chapman and Hall/CRC, 2011.
- [40] Y. Liu, X. Fan, C. Lv, J. Wu, L. Li, and D. Ding, "An innovative information fusion method with adaptive kalman filter for integrated ins/gps navigation of autonomous vehicles," *Mechanical Systems and Signal Processing*, vol. 100, pp. 605–616, 2018.
- [41] L. Jiang and H. Zhang, "Redundant measurement-based second order mutual difference adaptive kalman filter," *Automatica*, vol. 100, pp. 396– 402, 2019.
- [42] N. Kumar, B. Singh, B. K. Panigrahi, C. Chakraborty, H. M. Suryawan-shi, and V. Verma, "Integration of solar pv with low-voltage weak grid system: Using normalized laplacian kernel adaptive kalman filter and learning based inc algorithm," *IEEE Transactions on Power Electronics*, 2019
- [43] "Plexim Electrical Engineering Software," https://www.plexim.com.
- [44] "Opal-RT Technologies," https://www.opal-rt.com.